Letter

Acoustic corner state transfer mapping to synthetic higher-order topological semimetal

Hui Liu,[1,*] Haonan Wang,[1,*] Boyang Xie,[1] Hua Cheng,[1,†] Zhengyou Liu,[2,3,‡] and Shuqi Chen[1,4,5,§]

[1]*The Key Laboratory of Weak Light Nonlinear Photonics, Ministry of Education, School of Physics and TEDA Institute of Applied Physics, Nankai University, Tianjin 300071, China*

[2]*Key Laboratory of Artificial Micro- and Nanostructures of Ministry of Education and School of Physics and Technology, Wuhan University, Wuhan 430072, China*

[3]*Institute for Advanced Studies, Wuhan University, Wuhan 430072, China*

[4]*School of Materials Science and Engineering, Smart Sensing Interdisciplinary Science Center, Nankai University, Tianjin 300350, China*

[5]*The Collaborative Innovation Center of Extreme Optics, Shanxi University, Taiyuan, Shanxi 030006, China*

(Received 18 April 2022; revised 25 September 2023; accepted 28 September 2023; published 16 October 2023)

The robust transport of quantized particles in gap systems through adiabatic cyclic evolution corresponds to dynamical versions of topological insulators, which have recently emerged as a thriving topic. Until now, these connections were thought to be limited to gap systems. Here, we report a mechanism for corner state transfer in a gapless system, which arises as a synthetic higher-order Weyl semimetal. This is realized in the phononic version of a breathing kagome lattice, which is stacked layer by layer with weak interlayer couplings in the z direction, mimicking the time axis. We observed the corner state transfer, which hosts Weyl points and hinge states in synthetic three-dimensional (two-dimensional lattice+one-dimensional time) space. Our proposed corner states periodically undergo two topologically nontrivial phases along the time axis, resulting in the transport of the corner states, which corresponds to the switching of the two hinge states. Moreover, we experimentally demonstrated that the transport process is robust against defects. Our results provide insight into studying topological phases in synthetic space as well as an effective approach for manipulating acoustic waves.

DOI: 10.1103/PhysRevB.108.L161104

Introduction. A famous example of topological state transfer in synthetic dimensions is the topological pumping proposed by Thouless [1]. It supports edge modes spanning nontrivial band gaps with a time-modulated one-dimensional (1D) periodic potential. The topological bulk response of 1D topological pumping, characterized by nontrivial first Chern numbers, matches that of two-dimensional (2D) quantum Hall systems [2]. Generalizing the 1D topological pumping to 2D results in an additional quantized bulk response corresponding to the four-dimensional quantum Hall effect described by the second Chern number [3–5]. This edge state transfer maps dynamical phenomena to d-dimensional (dD) topological insulators (TIs), which host $(d-1)$D topological boundary states according to the bulk-boundary correspondence. The physics of topological pumping can be intrinsically investigated in condensed matter systems [6]. Additionally, this physics can be extended to classical systems, giving rise to a variety of extraordinary research in photonic [7–10], ultracold atomic systems [11,12], mechanical systems [13,14], elastic systems [15–18], and acoustics [19–22].

Recently, the concept of topological state transfer has been extended to higher-order topology [23], which fundamentally goes beyond the conventional bulk-boundary correspondence of conventional topology. According to the modern theory of polarization, a dD hth-order phase is characterized by the appearance of nontrivial boundary phenomena manifesting at its $(d-h)$D boundaries [24,25]. This novel physical concept of higher-order topology has opened up new avenues for investigating topological phases and associated topological states, including corner states and hinge states in higher-order topological insulators (HOTIs) [26] and higher-order topological semimetals (HOTSs) [27,28]. To date, a variety of higher-order topological phases, such as second-order TIs [29–31], third-order TIs [32,33], and second-order topological semimetals [34,35], have been demonstrated in various systems including electrical circuits, and photonic and acoustic systems. For a long time, research on topological state transfer has mainly focused on the dynamic counterpart of conventional TIs, with little attention paid to counterparts in higher-order topological phases. However, recent theoretical breakthroughs in higher-order topological pumping have shown that the higher-order state transfer in gapped systems is the dynamical realization of higher-order topology, bridging the relationship between topological state transfer and HOTIs [24,25]. A recent experimental realization of second-order topological pumping in photonic waveguides [23], corresponding to theoretically predicted HOTIs with chiral hinge states, has validated this concept. So far, most research on topological state transfer in first-order and higher-order topological systems has mainly focused on the insulator phases. As far as we know, higher-order topological state transfer does not involve counterparts in topological semimetals, which

*These authors contributed equally to this work.
†Corresponding author: hcheng@nankai.edu.cn
‡Corresponding author: zyliu@whu.edu.cn
§Corresponding author: schen@nankai.edu.cn

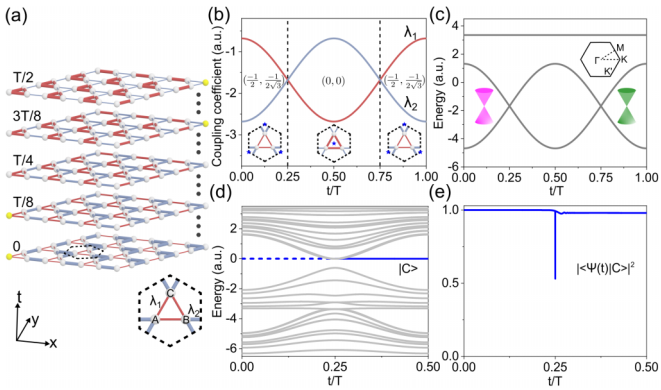

FIG. 1. Tight-binding model of corner state transfer without a gap. (a) Schematic illustration of corner state transfer. The yellow areas indicate the positions of the corner states. The inset shows a unit cell. (b) Two in-plane coupling coefficients as a function of t. Insets depict the Wannier centers denoted by blue stars. (c) The bulk dispersion at the K point along the t direction. The band gap between the lower two bands closes at $t = T/4$ and $t = 3T/4$, which correspond to Weyl points with opposite topological charges denoted by purple and green cones. The coupling parameters are $\phi_0 = 0$, $\lambda_0 = -1.68$, and $\delta = 1$. (d) The projected dispersion of the supercell along the t axis. (e) The evolution of the corner mode occupation probabilities for an interaction time $T = 10\,000$.

may provide an alternate approach to synthesize novel topological semimetals.

In this Letter, we report another mechanism for higher-order corner state transfer in gapless systems, which can be viewed as a HOTS in synthetic 3D (2D lattice + 1D time) space. This can be realized in a dynamic 2D kagome lattice, where the evolution of the corner mode from one corner to another experiences gap closing and reopening. We observed the corner state transfer in a phononic crystal by stacking 2D rhombic supercells in the z direction, where the in-plane couplings in each layer vary periodically along z, mimicking cyclic evolution with time. The topological phenomena in the 2D evolution process are rooted in the subtle higher-order Weyl semimetal phase. The gap closure in the evolution corresponds to the Weyl points with topological charges of ± 1. The trace of corner state transfer, supported by two distinct higher-order topological phases, maps to the switching of hinge states in the higher-order Weyl semimetal. The boundary states in each 2D layer can be viewed as time slices of surface states connecting Weyl points with opposite topological charges. We also observe the backscattering-immune properties for the corner state transfer. Our results provide a strategy to construct a relationship between topological state transfer and the HOTS phase, which can be exploited in the manipulation of acoustic waves.

Model and methods. Figure 1(a) depicts a schematic of corner state transfer using a tight-binding model, consisting of 2D rhombic supercells with evolving coupling along temporal space. The intracell couplings λ_1 (red tubes) and the intercell couplings λ_2 (blue tubes) continuously vary with time evolution in a half period, resulting in the transport of corner states from one corner to another. The corner state transfer experiences a gap closure corresponding to the Weyl point, which is a different mechanism from the well-recognized pumping process in gap systems. Viewing time as a virtual axis, the dynamic 2D kagome system appears as a higher-order Weyl semimetal in the synthetic 3D space. From the perspective of semimetal physics, the hinge states, which represent the trace of corner states along the time axis, can switch between two hinges when passing through the Weyl point.

We consider a unit cell of a 2D breathing kagome lattice, where A, B, and C denote three types of atoms. The three-band tight-binding Hamiltonian is given by

$$H(k_x, k_y, t) = \begin{pmatrix} 0 & h_{12} & h_{13} \\ h_{12}^* & 0 & h_{23} \\ h_{13}^* & h_{23}^* & 0 \end{pmatrix}, \tag{1}$$

where $h_{12} = \lambda_1 + \lambda_2 e^{-ik_x}$, $h_{13} = \lambda_1 + \lambda_2 e^{-i(k_x/2+\sqrt{3}k_y/2)}$, and $h_{23} = \lambda_1 + \lambda_2 e^{i(k_x/2-\sqrt{3}k_y/2)}$. $\lambda_1 = \lambda_0 + \delta\cos(\phi_0 + \frac{2\pi t}{T})$ and $\lambda_2 = \lambda_0 - \delta\cos(\phi_0 + \frac{2\pi t}{T})$ are the intracell and intercell couplings with cyclic time evolution. ϕ_0, λ_0, and δ represent the initial phase, unmodulated coupling, and modulation amplitude, respectively. The two in-plane couplings λ_1 and λ_2 are time-modulated cosine functions, as shown in Fig. 1(b). In one cycle, the band gap will close at $t = T/4$ and $t = 3T/4$ denoted by black dashed lines, indicating the phase transitions.

The topological properties of the kagome lattice are characterized by bulk polarization,

$$P_i = -\frac{1}{S}\iint_{\mathrm{BZ}} A_i d^2k, \quad i = x, y, \tag{2}$$

where $A_i = -i\langle u|\partial_{k_i}|u\rangle$ is the Berry connection, $|u\rangle$ is the Bloch wave function, and S represents the area of the first Brillouin zone (BZ). The position of the Wannier center can be determined by the bulk polarization (P_x, P_y) as a function of t. The evolution undergoes two distinct topological phases, which are determined by the bulk polarization $(-1/2, -1/2\sqrt{3})$ for $|t - T/2| > T/4$ and (0,0) for $|t - T/2| < T/4$. The Wannier centers are located at two different locations in the unit cell, as shown in the insets of Fig. 1(b). The band structure at the high-symmetry point K as a function of t is shown in Fig. 1(c), where the band gap of the lower two bands will close at $t = T/4$ and $t = 3T/4$, carrying opposite topological charges denoted by cones with different colors. The bulk state dispersions are linear along all three directions near the twofold degenerate points, corresponding to Weyl points. The dispersion of the time-dependent rhombic supercell in a half period is shown in Fig. 1(d). The corner eigenmode $|C\rangle$ shifts its distribution along the t axis with the gap closing and reopening, where the opposite distribution is denoted by blue dashed and solid lines. The evolution process can be described by the Schrödinger equation $i\frac{\partial}{\partial t}\psi(t) = H(t)\psi(t)$, where $\psi(t)$ is the transient state. After expanding the transient state as the superposition of the eigenmode at a given t value, the evolution of corner mode occupation probabilities $|a_C(t)|^2 = |\langle\psi(t)|C\rangle|^2$ can be obtained, as shown in Fig. 1(e). The transfer rate of the corner state from one corner to another is close to one, similar to a pumping process. However, the process is nonadiabatic due to the inevitable transition to the bulk state at the gap closure moment. The

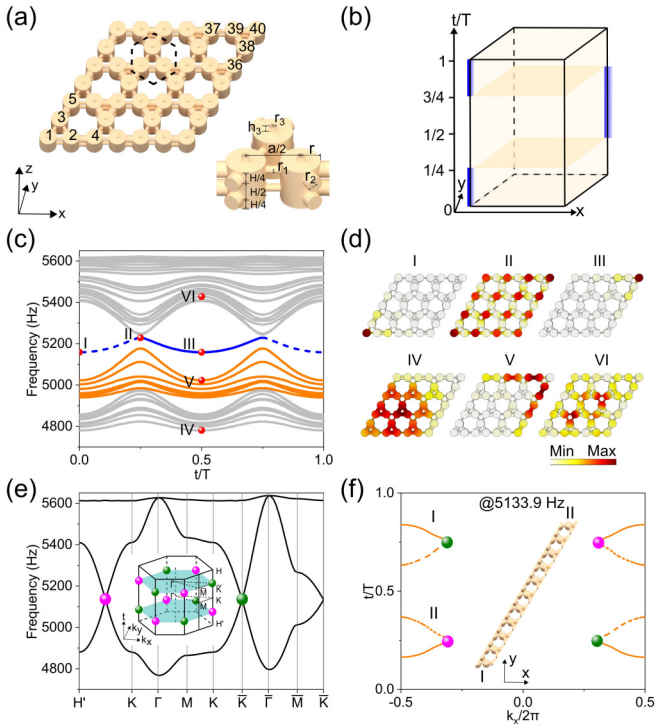

FIG. 2. Acoustic corner state transfer exhibiting HOTS properties. (a) 2D time-modulated acoustic crystal and its unit cell. (b) Schematic of the periodical distributions of hinge states denoted by blue lines. (c) The projected dispersion along the time direction. (d) Acoustic eigenpressure fields for bulk states (II, IV, VI), surface states (V), and hinge states (I, III) corresponding to the eigenfrequency at the given t value in (c). (e) Bulk state dispersion of the unit cell. The inset shows the first BZ, where purple and green spheres represent Weyl points with charges of $+1$ and -1 at $t = T/4$ and $t = 3T/4$. (f) The Fermi arcs connect Weyl points with opposite charges on the I and II surfaces, represented by solid and dashed lines, respectively. The frequency of Weyl points is set to 5133.9 Hz.

high transfer rate is rooted in the subtle high-order Weyl semimetal phase in the synthetic space. Since the gap closing and reopening with time conforms to a Weyl point, the density of states is minimal, leading to a minimal transition to the bulk states and a high transfer rate to the corner state on the opposite corner.

To implement the scenario described above, we construct a phononic crystal where the in-plane couplings in 2D kagome lattices vary periodically with time. We consider a dynamic 2D rhombic supercell with a 3×3 unit cell as shown in Fig. 2(a), where acoustic cavities are labeled from 1 to 40. The inset shows the unit cell of the supercell with a lattice constant of $a = 81$ mm, containing three cavities with $H = 34$ mm and $r = 15$ mm corresponding to A, B, and C atoms. The intracell couplings with $r_1 = r_0 - \delta\cos(\phi_0 + \frac{2\pi t}{T})$ and intercell couplings with $r_2 = r_0 + \delta\cos(\phi_0 + \frac{2\pi t}{T})$ of each layer are periodically modulated as a function of cyclic time evolution t, where $r_0 = 5.2$ mm and $\delta = 2.2$ mm. The dynamic phononic crystal corresponds well with the tight-binding model, as shown in Supplemental Material Sec. I [36]. Accurate design ensures that only one of the acute angles of the supercell can pass through the Wannier centers in distinct topological phases, making the higher-order corner states exist only at the first or 40th atom. The corner state distribution along the time axis, mapping to the hinge state, is consistent with the results of the tight-binding model, as shown in Fig. 2(b). By using time acting as a bridge, we can connect a conventional 2D higher-order insulator response with 3D HOTS. If we view the t axis as a virtual dimension, the topological phenomena in the dynamic 2D rhombic supercell can be understood through semimetal physics. Figure 2(c) shows the full dispersion of all the states from the perspective of synthetic HOTS, including the hinge, surface, and bulk states, denoted by blue, orange, and gray lines, respectively. The states will undergo the band closing and reopening process, where two hinge states exist in the range of $|t - T/2| > T/4$ and $|t - T/2| < T/4$, represented by blue dashed and solid lines, respectively. Correspondingly, the simulated acoustic eigenpressure fields for the bulk (II, VI, IV), surface (V), and hinge (I, III) at given t values, are shown in Fig. 2(d). The slice of the hinge state along the t axis is equivalent to the corner state at a given t. Thus, the corner state transfer is the result of the hinge state switch in synthetic HOTS. It is worth noting that no corner state transfer is possible in existing HOTSs, as they pass through topologically trivial and nontrivial phases along the k_z direction, and the hinge state only exists in a specific k_z range.

The higher-order Weyl semimetal properties in the evolution of corner states can be further confirmed by analyzing the bulk band structure and Fermi arcs. The simulated bulk band structure of high-symmetric lines shows two linear two-band crossings at $K_\pm = (4\pi/3a, 0, \pm T/4)$, which correspond to Weyl points with opposite charges as shown in Fig. 2(e). The first BZ in the inset of Fig. 2(e) presents the distribution of Weyl points, where the time-reversal counterparts are $K'_\pm = (-4\pi/3a, 0, \pm T/4)$. The purple and green spheres indicate the Weyl points with opposite topological charges of ± 1. The details of topological charges determined by the Wilson loop at the degeneracy point are shown in Supplemental Material Sec. II [36]. Fermi arcs connecting the projections of Weyl points with opposite topological charges at the Weyl point frequency are clearly revealed in Fig. 2(f) when considering the surface states in a ribbon. The hallmarks of a synthetic higher-order Weyl semimetal, i.e., hinge states, Weyl points, and Fermi arcs, can be found in the evolution of corner states.

Since time-dependent intralayer coupling is difficult to achieve in acoustic systems, we use the z axis to take over the role of time in the experiment. We tested the aforementioned prediction by constructing a 3D phononic crystal. This crystal consists of dynamic 2D rhombic supercells that were stacked layer by layer with weak interlayer couplings in the z direction, mimicking the time axis. The interlayer coupling tubes ($r_3 = 3$ mm and $h_3 = 4$ mm) established a decoupled vertical transmission channel for sound waves. Different from the weakly coupled photonic waveguides which can match well with the time-dependent model, the major difference is the discrete character of the z axis and the interlayer couplings in acoustics, resulting in a variation of k_z. To obtain the dispersion of a 3D phononic crystal as a function of k_z and t, we impose periodic boundary conditions to each layer in the acoustic system that horizontal coupling varies slowly

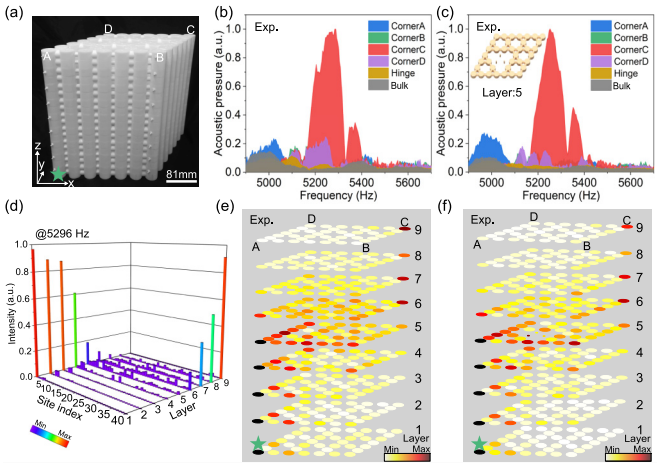

FIG. 3. Observation of the corner state transfer. (a) Photograph of the 3D-printed sample. The green star indicates the location of the sound source. (b), (c) Measured acoustic pressure spectra at the final layer for the sample without defects and with defects, respectively. The inset of (c) shows the defects in the fifth layer. (d) Measured pressure intensity for corner state evolution with different layers at 5296 Hz. (e), (f) Measured pressure distributions for the sample without defects and with defects at 5296 Hz, respectively.

along the z direction. The equifrequency trajectory of the corner state $k_z(t)$ can be visualized when a fixed frequency of 5296 Hz is selected to cross the dispersion surfaces. This means that the corner state in each discrete layer hosting different k_z can be excited at 5296 Hz. The details are given in Supplemental Material Sec. III [36].

Experimental realization of a synthetic HOTS. To observe the corner state evolution process, we selected nine discrete layers to ensure a high corner state transfer rate and minimize acoustic attenuation caused by transmission distance (Supplemental Material Secs. IV and V [36]). The sample composed of nine stacking rhombic structures fabricated by a 3D printing technique is shown in Fig. 3(a). The top and bottom of the sample are set to the absorbing boundary conditions to minimize internal reflections and outside interference. The corner state is excited by a source represented by a green star in the initial layer and transfers layer by layer until it is finally absorbed at the top of the sample. A microphone was inserted into the sample to probe the acoustic pressure signal. The measured acoustic pressure spectra in the final layer are shown in Fig. 3(b). The acoustic pressure for the boundary and bulk mode is obtained by averaging the pressure of all the cavities at the edge and bulk. The sound intensity is concentrated at corner C opposite to the excitation source, and suppressed at other positions near 5296 Hz, indicating the corner state evolves from the excited source to the opposite corner. The robustness of the corner state transfer was also observed by removing a unit cell in the fifth layer of the sample. The measured acoustic pressure spectra with the defects are shown in Fig. 3(c), which shows similar results to Fig. 3(b), proving the robustness of the corner state transfer against defects. The experimental results match well with the simulated results in Supplemental Material Sec. VI [36].

The pressure distributions of the corner mode evolution at 5296 Hz are shown in Fig. 3(d) for the sample without defects. The acoustic pressure is excited at the first cavity in the first layer, then evolves into the bulk at the middle, and gradually transfers to the 40th cavity (corner C) in the ninth layer. The measured spatial distributions of acoustic pressure at 5296 Hz are shown in Fig. 3(e), intuitively displaying the evolution process of corner states. The evolution of corner states forms hinge states along the z direction, with layers 1–4 on one hinge and layers 6–9 on another, which corresponds to a synthetic HOTS. The evolution undergoes two distinct topological phases leading to the opposite distributions of hinge states, where the gap closes and a phase transition occurs in the middle layer. Although the evolution is nonadiabatic and inevitably affected by sound loss, the corner state transfer can still be completed. The measured transfer rate of the corner state is close to one, which is consistent with the theoretical model. Further details are provided in Supplemental Material Sec. IV [36]. We also observed the spatial pressure distributions with defects at 5296 Hz, as shown in Fig. 3(f), where the corner state transmits smoothly around the defects. The robustness of the corner state transfer against the defects in different layers is illustrated in Supplemental Material Sec. VII [36]. All the measured results match the theoretical and simulated results, demonstrating the realization of the corner state transfer and its counterpart, i.e., the hinge states.

Conclusions. In conclusion, we designed and fabricated a phononic crystal to demonstrate the corner state transfer, which can be viewed as a dynamical realization of a novel 3D second-order topological semimetal. The corner state evolution undergoes the processes of gap closing and reopening as the in-plane coupling varies along the z direction, mimicking the time axis. We found the key features of a higher-order Weyl semimetal, including Weyl points, hinge states and surface states, in the evolution process. We observed the corner state transfer and its counterpart, i.e., the switching of the two hinge states in a higher-order Weyl semimetal. Furthermore, we experimentally verified the robustness of the transport against defects. Our work is distinct from earlier works on topological state evolution mainly reflected in a surprising correspondence between low-dimensional dynamic systems and high-dimensional semimetals. The corner state transfer spanning two distinct topological phases in temporal space is a mechanism for HOTS that is difficult to achieve for usual topological semimetals that rely on k_z modulation. This work provides insights into the connections between different topological systems, which can be further explored in other systems, such as photonic systems and elastic systems.

Acknowledgment. This work was supported by the National Key Research and Development Program of China (2022YFA1404501 and 2021YFA1400601), the National Natural Science Fund for Distinguished Young Scholars (11925403), and the National Natural Science Foundation of China (Grants No. 12122406, No. 12192253, No. 12304486, and No. 12004198).

[1] D. J. Thouless, Quantization of particle transport, Phys. Rev. B **27**, 6083 (1983).

[2] H. Q. Zhou, S. Y. Cho, and R. H. McKenzie, Gauge fields, geometric phases, and quantum adiabatic pumps, Phys. Rev. Lett. **91**, 186803 (2003).

[3] Y. E. Kraus, Z. Ringel, and O. Zilberberg, Four-dimensional quantum hall effect in a two-dimensional quasicrystal, Phys. Rev. Lett. **111**, 226401 (2013).

[4] O. Zilberberg, S. Huang, J. Guglielmon, M. Wang, K. P. Chen, Y. E. Kraus, and M. C. Rechtsman, Photonic topological boundary pumping as a probe of 4D quantum Hall physics, Nature (London) **553**, 59 (2018).

[5] M. Lohse, C. Schweizer, H. M. Price, O. Zilberberg, and I. Bloch, Exploring 4D quantum Hall physics with a 2D topological charge pump, Nature (London) **553**, 55 (2018).

[6] M. Switkes, C. M. Marcus, K. Campman, and A. C. Gossard, An adiabatic quantum electron pump, Science **283**, 1905 (1999).

[7] Y. E. Kraus, Y. Lahini, Z. Ringel, M. Verbin, and O. Zilberberg, Topological states and adiabatic pumping in quasicrystals, Phys. Rev. Lett. **109**, 106402 (2012).

[8] L. Wang, M. Troyer, and X. Dai, Topological charge pumping in a one-dimensional optical lattice, Phys. Rev. Lett. **111**, 026802 (2013).

[9] Z. Fedorova, Q. Haixin, S. Linden, and J. Kroha, Observation of topological transport quantization by dissipation in fast Thouless pumps, Nat. Commun. **11**, 3758 (2020).

[10] M. Jürgensen, S. Mukherjee, and M. C. Rechtsman, Quantized nonlinear Thouless pumping, Nature (London) **596**, 63 (2021).

[11] M. Lohse, C. Schweizer, O. Zilberberg, M. Aidelsburger, and I. Bloch, A Thouless quantum pump with ultracold bosonic atoms in an optical superlattice, Nat. Phys. **12**, 350 (2016).

[12] S. Nakajima, T. Tomita, S. Taie, T. Ichinose, H. Ozawa, L. Wang, M. Troyer, and Y. Takahashi, Topological thouless pumping of ultracold fermions, Nat. Phys. **12**, 296 (2016).

[13] I. H. Grinberg, M. Lin, C. Harris, W. A. Benalcazar, C. W. Peterson, T. L. Hughes, and G. Bahl, Robust temporal pumping in a magneto-mechanical topological insulator, Nat. Commun. **11**, 974 (2020).

[14] Y. Xia, E. Riva, M. I. N. Rosa, G. Cazzulani, A. Erturk, F. Braghin, and M. Ruzzene, Experimental observation of temporal pumping in electromechanical waveguides, Phys. Rev. Lett. **126**, 095501 (2021).

[15] M. I. N. Rosa, R. K. Pal, J. R. F. Arruda, and M. Ruzzene, Edge states and topological pumping in spatially modulated elastic lattices, Phys. Rev. Lett. **123**, 034301 (2019).

[16] E. Riva, M. I. N. Rosa, and M. Ruzzene, Edge states and topological pumping in stiffness-modulated elastic plates, Phys. Rev. B **101**, 094307 (2020).

[17] H. Chen, L. Y. Yao, H. Nassar, and G. L. Huang, Mechanical quantum Hall effect in time-modulated elastic materials, Phys. Rev. Appl. **11**, 044029 (2019).

[18] E. Riva, G. Castaldini, and F. Braghin, Adiabatic edge-to-edge transformations in time-modulated elastic lattices and non-Hermitian shortcuts, New J. Phys. **23**, 093008 (2021).

[19] Y. X. Shen, Y. G. Peng, D. G. Zhao, X. C. Chen, J. Zhu, and X. F. Zhu, One-way localized adiabatic passage in an acoustic system, Phys. Rev. Lett. **122**, 094501 (2019).

[20] W. Cheng, E. Prodan, and C. Prodan, Experimental demonstration of dynamic topological pumping across incommensurate bilayered acoustic metamaterials, Phys. Rev. Lett. **125**, 224301 (2020).

[21] Z.-G. Chen, W. Tang, R.-Y. Zhang, Z. Chen, and G. Ma, Landau-Zener transition in the dynamic transfer of acoustic topological states, Phys. Rev. Lett. **126**, 054301 (2021).

[22] H. Chen, H. Zhang, Q. Wu, Y. Huang, H. Nguyen, E. Prodan, X. Zhou, and G. Huang, Creating synthetic spaces for higher-order topological sound transport, Nat. Commun. **12**, 5028 (2021).

[23] W. A. Benalcazar, J. Noh, M. Wang, S. Huang, K. P. Chen, and M. C. Rechtsman, Higher-order topological pumping and its observation in photonic lattices, Phys. Rev. B **105**, 195129 (2022).

[24] W. A. Benalcazar, B. A. Bernevig, and T. L. Hughes, Quantized electric multipole insulators, Science **357**, 61 (2017).

[25] W. A. Benalcazar, B. A. Bernevig, and T. L. Hughes, Electric multipole moments, topological multipole moment pumping, and chiral hinge states in crystalline insulators, Phys. Rev. B **96**, 245115 (2017).

[26] F. Schindler, A. M. Cook, M. G. Vergniory, Z. Wang, S. S. Parkin, B. A. Bernevig, and T. Neupert, Higher-order topological insulators, Sci. Adv. **4**, eaat0346 (2018).

[27] M. Lin and T. L. Hughes, Topological quadrupolar semimetals, Phys. Rev. B **98**, 241103(R) (2018).

[28] M. Ezawa, Higher-order topological insulators and semimetals on the breathing kagome and pyrochlore lattices, Phys. Rev. Lett. **120**, 026801 (2018).

[29] M. Serra-Garcia, V. Peri, R. Süsstrunk, O. R. Bilal, T. Larsen, L. G. Villanueva, and S. D. Huber, Observation of a phononic quadrupole topological insulator, Nature (London) **555**, 342 (2018).

[30] H. Xue, Y. Yang, F. Gao, Y. Chong, and B. Zhang, Acoustic higher-order topological insulator on a kagome lattice, Nat. Mater. **18**, 108 (2019).

[31] S. Mittal, V. V. Orre, G. Zhu, M. A. Gorlach, A. Poddubny, and M. Hafezi, Photonic quadrupole topological phases, Nat. Photon. **13**, 692 (2019).

[32] H. Xue, Y. Ge, and H.-X. Sun, Observation of an acoustic octupole topological insulator, Nat. Commun. **11**, 2442 (2020).

[33] S. Liu, S. Ma, Q. Zhang, L. Zhang, C. Yang, O. You, W. Gao, Y. Xiang, T. J. Cui, and S. Zhang, Octupole corner state in a three-dimensional topological circuit, Light: Sci. Appl. **9**, 145 (2020).

[34] Q. Wei, X. Zhang, W. Deng, J. Lu, X. Huang, M. Yan, G. Chen, Z. Liu, and S. Jia, Higher-order topological semimetal in phononic crystals, Nat. Mater. **20**, 812 (2021).

[35] L. Luo, H. X. Wang, Z. K. Lin, B. Jiang, Y. Wu, F. Li, and J. H. Jiang, Observation of a phononic higher-order Weyl semimetal, Nat. Mater. **20**, 794 (2021).

[36] See Supplemental Material at http://link.aps.org/supplemental/10.1103/PhysRevB.108.L161104 for (I) comparison between the tight-binding model and finite-element method, (II) topological charge of the Weyl points, (III) dispersion of a three-dimensional phononic crystal, (IV) corner state transfer rate, (V) intensity and transmission for a corner state mode with different discrete layers, (VI) simulated corner state transfer, and (VII) corner state transfer with defects in different layers, which includes Refs. [37–41].

[37] A. A. Soluyanov, D. Gresch, Z. Wang, Q. Wu, M. Troyer, X. Dai, and B. A. Bernevig, Type-II Weyl semimetals, Nature (London) **527**, 495 (2015).

[38] H. X. Wang, G. Y. Guo, and J. H. Jiang, Band topology in classical waves: Wilson-loop approach to topological numbers and fragile topology, New J. Phys. **21**, 093029 (2019).

[39] S. Longhi, Topological pumping of edge states via adiabatic passage, Phys. Rev. B **99**, 155150 (2019).

[40] Z. Wang, Y. Chong, J. D. Joannopoulos, and M. Soljačić, Observation of unidirectional backscattering-immune topological electromagnetic states, Nature (London) **461**, 772 (2009).

[41] B. Xie, H. Liu, H. Wang, H. Cheng, J. Tian, Z. Liu, and S. Chen, Tailoring the surface and interface states in a three-dimensional fragile topological insulator with kagome lattice, Phys. Rev. B **106**, 115305 (2022).